Nonlinear Acoustic Behavior Prediction and Analysis of Straight Through Perforated Tube Silencer With Flow

Kangjian Han and Zhenlin Ji

School of Power and Energy Engineering, Harbin Engineering University, Harbin, Heilongjiang, 150001, P.R. China. E-mail: Hankangjian_heu@163.com

(Received 22 August 2023; accepted 22 January 2024)

Straight through perforated tube silencers are widely used in intake and exhaust noise control, and their acoustic behaviors are influenced by the gas flow and high amplitude sound remarkably. To investigate the acoustic attenuation performance of straight through perforated tube silencers in the presence of flow and high amplitude sound, an approach based on the three-dimensional (3D) time-domain computational fluid dynamics (CFD) simulation is employed and validated by comparing predictions and measurements. Transmission loss of the straight through perforated tube silencer under pure tone and multi-tone sound excitations is predicted. Results show that, under the pure tone sound excitations, the acoustic attenuations are affected remarkably by the high amplitude sound, and the nonlinear effects turn to weaken as flow velocity increases. With the sound pressure level (SPL) decreasing along the axis of the silencer, the acoustic nonlinearity in the orifice weakens gradually. The shedding vortices are restricted to the region near perforations because of the transport of flow. When the multi-tone sound excitation is enforced on the inlet, transmission loss of the silencer is different from the pure tone excitation at the same SPL of every compositional frequency.

1. INTRODUCTION

Silencers are widely used to eliminate unwanted noise[1] in the intake and exhaust system of turbocharged internal combustion engines. For straight through perforated tube silencers, the air flow may graze across the orifices and the high SPL may induce acoustic nonlinearity in the orifices, thereby impacting the acoustic attenuation performance of the silencer.[2] Due to the effects of grazing flow and high-amplitude sound, predicting the transmission loss of the perforated tube silencers using frequency-domain methods is difficult.[3–5]

Goldman[6] measured the acoustic impedance of circular orifices under the turbulent boundary layer, and found that the acoustic impedance of circular orifices with grazing flow is markedly affected by the high amplitude sound, the nonlinear effect gradually weakens with increasing flow velocity, and the influence of turbulent flow on the acoustic impedance is inapparent at high SPL. In the investigations of honeycomb acoustic liners, Zhang and Bodony[7,8] found that, when a high amplitude sound wave propagates in the orifice, shedding vortices periodically appear at the edges. When the grazing flow is present, the transport of flow significantly affects the propagation of shedding vortices, and the turbulent boundary layer near the orifice is destroyed by the high particle velocity. Chen et al.[9] found that the SPL in the duct gradually decreases and the acoustic nonlinearity of the orifice gradually weakens as the location of orifices goes further from the inlet in a lined tube. Therefore, the complex acoustic characteristics of the orifice pose the demand for accurate methods to predict the acoustic attenuation behavior of perforated tube silencers in the presence of flow and high amplitude sound.

Sullivan[10] presented a simple one-dimensional (1D) method based on the four-pole parameters of different elementary segments to predict the nonlinear transmission loss of perforated tube silencers. Dickey et al.[11] employed the 1D time-domain finite difference method to study the nonlinear attenuation behaviors of perforated tube silencers. In Sulivan's[10] and Dickey's[11] works, the orifices were characterized by the acoustic impedance expressions acquired from measurements in the absence of flow. For the cases with flow, Chang and Cummings[12] employed a differential equation to describe the nonlinear acoustic characteristics of the orifice and solved the quasi-1D equations governing the sound field in time domain by using the finite difference method to determine the transmission loss of perforated tube silencers under the high amplitude pulse sound excitations. El-Rahman et al.[13] studied the nonlinear effects on the acoustic attenuation performance of perforated tube silencers by solving the quasi-1D compressible flow equations and adopting a suitable effective length correction for the orifice to consider the nonlinear effects. The above mentioned studies are limited to the 1D sound propagation and exclude the 3D wave effects which may lead especially to inaccurate predictions at higher frequencies. The restrictions of the acoustic impedance formulas and the mean flow assumption employed in above literatures further limit the application of the 1D methods.

Several researchers employed numerical methods to determine the acoustic behavior of resonators by solving the Reynolds averaged Navier-Stokes (RANS) equations,[14–23] or the Navier-Stokes (N-S) equations.[7,8,24] Broatch et al.[14] proposed an approach based on the CFD simulation to predict the transmission loss of expansion chamber silencers. Ji et al.[15–17] employed the 3D time-domain CFD approach to determine the acoustic attenuation behavior of perforated tube silencers under the low amplitude sound excitations by solving RANS equations, and the predictions were in good agreements with the measurements. Tam et al.[18] studied the acoustic character-

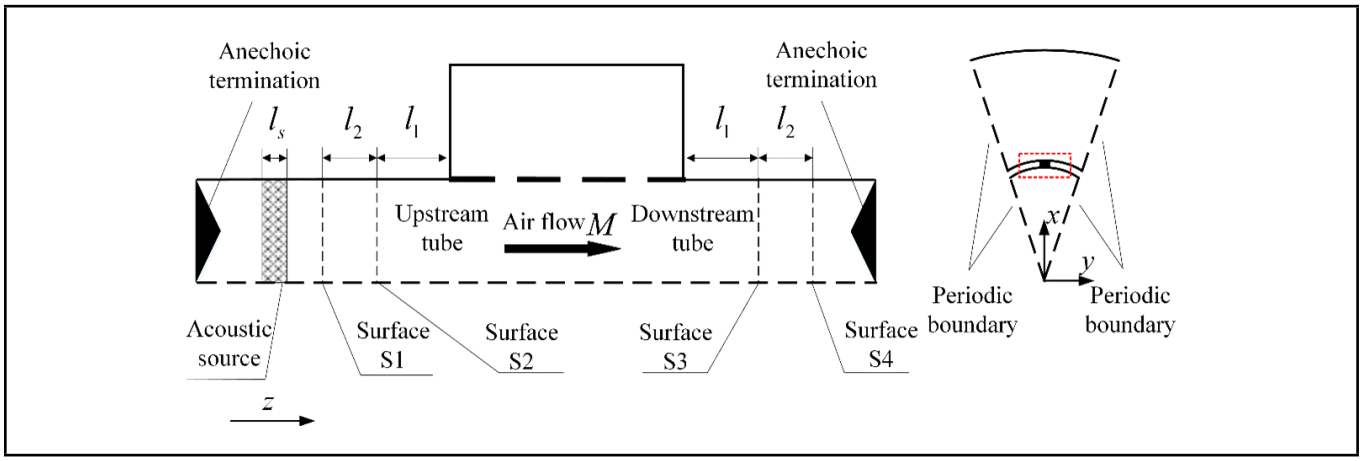

Figure 1. Computational model.

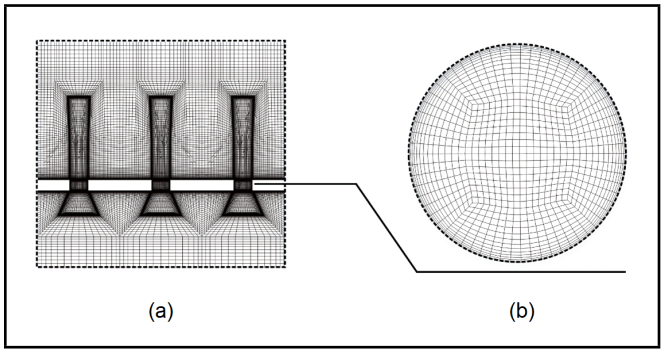

Figure 2. Discretized grids around the perforations.

istics of the acoustic liner with grazing flow and high amplitude sound excitations by solving the RANS equations. Their investigations indicated that the acoustic characteristics of the orifice could be simulated by solving the RANS equations. Liu et al.[21–23] successfully employed the 3D time-domain CFD approach to determine the insertion loss and noise reduction of the silencer. The above investigations showed that the 3D time-domain CFD approach has the advantages of considering the influences of viscosity, nonlinearity, 3D wave and turbulent flow, as well as low numerical dispersion in the acoustic computations. Zhang et al.[7,8] and Roche et al.[24] investigated the acoustic behavior of 3D acoustic liners with grazing flow and high SPL excitations by using the direct numerical simulation (DNS), and their predictions aligned with the measurements. However, the disadvantage of the DNS method is the huge computational resource consumption. Therefore, it is well-founded to conclude that the 3D time-domain CFD approach is suitable to predict the nonlinear acoustic behavior of the perforated tube silencer in the presence of flow and under high amplitude sound excitations.

In the present study, the 3D time-domain CFD approach by solving RANS equations is employed to predict transmission loss of the straight through perforated tube silencer under high amplitude sound excitations. The details of computational method and grid meshing are introduced in Section 2. Section 3 presents the measurement of transmission loss and validation of the present approach. The transmission loss predictions of straight through perforated tube silencers under the high amplitude pure tone and multi-tone sound excitations with different Mach number are discussed in Section 4. Finally, the study is concluded with final remarks in Section 5.

2. COMPUTATIONAL METHOD

2.1. Computational Model

In the present works, the sharp-edge circular orifices are uniformly distributed in the circumferential direction of a center tube in the straight through perforated tube silencer (shortened to 'perforated tube silencer' below). In order to reduce the computation time and consider the interaction among adjacent orifices, single symmetric unit and the rotational periodic boundary condition are adopted to predict transmission loss of perforated tube silencers.[15–17] The computational model is depicted in Fig. 1.

Upstream and downstream of the silencer are provided with a sufficiently long computational domain, and two side faces are set as the rotational periodic boundary. The anechoic terminations are applied at the inlet and outlet of the computational domain. A zone near the inlet, with a length of l_s, is selected as a virtual sound source to provide sound excitations. Four monitoring surfaces perpendicular to the flow are selected in the upstream and downstream computational domains, respectively. The mean Mach number in the center tube is M.

In the range of incident SPL studied in the present works, it is assumed that the acoustic nonlinearity only appears near the orifice, and plane sound wave propagates in the upstream and downstream tubes satisfying the linear acoustic equation.[2] The incident sound pressure p_i and transmitted sound pressure p_t can be related respectively as:[1]

$$p_i = \frac{p_{S2} - p_{S1}e^{jkl_2/(1-M)}}{e^{-jkl_2/(1+M)} - e^{jkl_2/(1-M)}}; \tag{1}$$

$$p_t = \frac{p_{S4} - p_{S3}e^{jkl_2/(1-M)}}{e^{-jkl_2/(1+M)} - e^{jkl_2/(1-M)}}; \tag{2}$$

where p_{Sn} is the area-weighted average sound pressure on monitoring surface Sn $(n = 1, 2, 3, 4)$, $k = 2\pi f/c$ is the wave number, f is the frequency, c is the sound speed, $l_2 = 30$ mm is the distance between the monitoring surfaces, $j = \sqrt{-1}$ is the imaginary unit. In order to minimize the influence of local perturbations of flow and nonplanar wave on predictions of transmission loss, the distance between monitoring surfaces and silencer, l_1, is set as 100 mm.

Transmission loss of the silencer may be expressed as:

$$TL = 10\log\left(\left|\frac{p_i}{p_t}\right|^2\right). \tag{3}$$

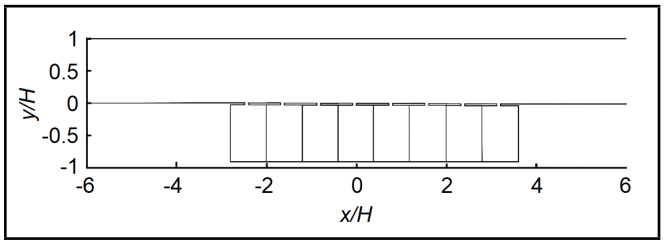

Figure 3. Schematic of the acoustic liner (H is the height of the channel).

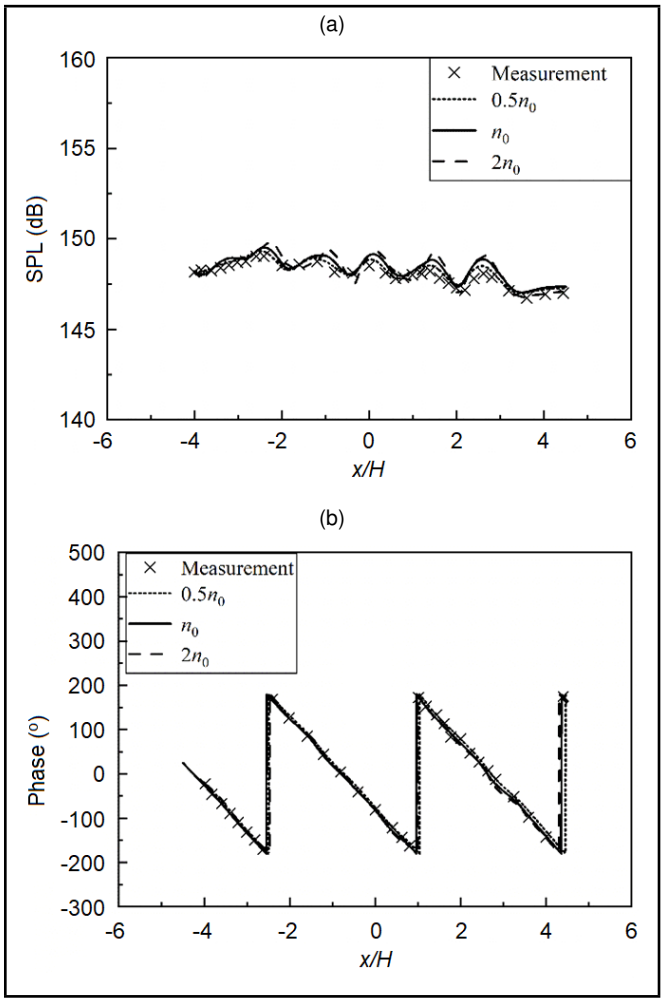

Figure 4. Grid independence study: (a) SPL, (b) phase.

2.2. Computational Scheme and Evaluation Method

The CFD commercial software Fluent[25] is employed to solve the N-S equations, and the laminar model is selected for the cases without flow, while the SST k-ω turbulence model is applied for the cases with flow. The Bounded Second Order Implicit stable transient formulation is chosen for the time-domain computation, and the time step is set to 5×10^{-6} s. SIMPLE (Semi-Implicit Method for Pressure-Linked Equations) pressure-velocity coupling algorithm is used in the steady flow simulation, and PISO (Pressure Implicit with Splitting of Operators) scheme is adopted for the transient computation. The second order upwind spatial discretization is applied to solve the mass, momentum, and energy equations. The working medium is air, and its density meets the ideal gas law.

The mass-flow-inlet and pressure-outlet conditions are set at the inlet and outlet of the computational model, respectively. And the selection box of non-reflecting boundary condition is checked[17] in transient computation. Walls of the model are set as the adiabatic wall boundary condition with no-slip, and heat exchange of the walls are not taken into account. Side boundaries of the computational domain are set as the rotational periodic boundary. A region near left terminal of the computational domain is set as the momentum source,[26] the sound signal is expressed as:

$$p(t) = \frac{l_s}{2}\psi(t); \tag{4}$$

where $\psi(t)$ is the intensity of the momentum source.

The simulation process of transmission loss of the perforated tube silencers can be summarized as follows: The target sound signal is continuously enforced at the sound source, and time histories of the area-weighted average sound pressures on monitoring surfaces S1-S4 are recorded, respectively. Then the acoustic signals in time domains are transformed into frequency domains using the fast Fourier transform (FFT). Finally, transmission loss is calculated by using Eqs. (1)-(3).

2.3. Computational Grid

In order to reduce the numerical dispersion and accelerate the convergence of simulations, the structured hexahedral grids are used to discretize the computational domain. When high amplitude sound propagates around perforations, the shedding vortices are generated at the edge of orifices.[7] Therefore, the grids near the orifices (the red dotted block in Fig. 1) need to be refined, as shown in Fig. 2(a). Figure 2(b) is the discretized grids on the cross-section of the orifices. To ensure enough grids, a trapezoidal zone with high-density grids is formed between the orifices and main tube. The viscosity-affected thickness of the orifice wall is $2\sqrt{\pi\mu/(\rho f)}$,[27] where μ is the dynamic viscosity coefficient of air, ρ is the density of air. Ten layers of grids are used to discretize the viscosity-affected region in the present works, and the first internal grid point is placed at $y+ \sim 1$ at the no-slip walls. In the computational domain far away from the orifices, the maximum axial size of grids is 1 mm, and the maximum growth rate in transitional area is 1.1.

The sound field of the acoustic liner,[18] as shown in Fig. 3, is simulated to analyze the grid independence for the following reasons: 1) Similar to the straight through perforated tube silencer, the flow grazes across the silts in the acoustic liner; 2) The grid independence is mainly performed for the grids around the orifices which have significant influence on the numerical computation. To make the grid independence more convincing, the grids consistent with Fig. 2(a) are adopted to discretize the slits. The mean Mach number in the channel is 0.3. On the basis of the above meshing scheme (assuming the number of grids is n_0), the number of grids is uniformly halved and doubled, respectively. Figure 4 shows the effect of grid quantity on the streamwise distribution of SPL and the relative phase along the wall opposite the liner under incident sound of 2000 Hz and 148.6 dB SPL (The measurement and extraction method of SPL and phase are presented in literature[18]). The results indicate that the meshing scheme in the present works has adequate numerical accuracy to simulate the sound field under high SPL excitations and in the presence of flow.

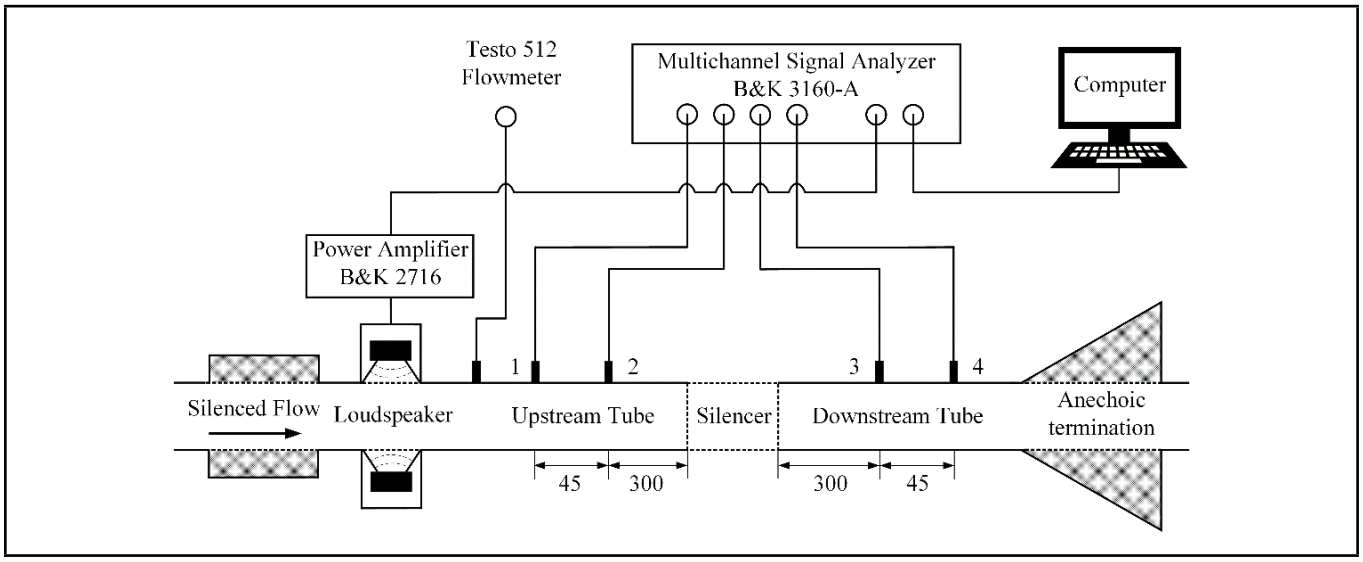

Figure 5. Schematic of the measurement set-up (unit: mm).

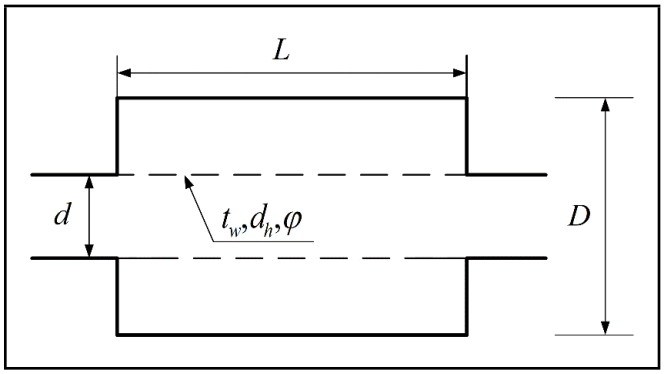

Figure 6. The diagram of perforated tube silencer.

3. MEASUREMENT AND VALIDATION

3.1. Measurement

The measurement set-up for transmission loss is shown in Fig. 5. The measured silencer is installed in the impedance tube with a 50 mm inner diameter. For both sides of the measured silencer, two PCB 377B26 probe microphones are mounted on the tube wall, with a distance of 45 mm, corresponding to the effective frequency range from 400 Hz to 2500 Hz.[28] The impedance tube is equipped with a tapered non-reflective terminal to minimize the reflected signal at the outlet, and a silencer to reduce the flow noise at the inlet. The multichannel signal analyzer is used to generate sound signals and provide the signal to the power amplifier to drive the loudspeakers as well as collect the signals of the four probe microphones. The Testo 512 flowmeter is used to acquire the flow velocity in the tube. The ambient temperature is 296 K.

3.2. Validation

The diagram of perforated tube silencers is shown in Fig. 6, where D and L are the diameter and length of the expansion chamber, respectively, d is the diameter of perforated tube, and t_w, d_h and φ are the wall thickness, orifice diameter and porosity of the perforation, respectively. The dimensions of the perforated tube silencers are listed in Table 1. The linear acoustic attenuation behaviors of perforated tube silencers are obtained at the SPL below 110 dB in the present study.

Table 1. Geometric parameters of the perforated tube silencers.

Silencer	D (mm)	L (mm)	d (mm)	t_w (mm)	d_h (mm)	φ
S-1	80	200	50	2	4.1	0.8%
S-2	63.5	254	26.6	3.4	3.18	3.97%
S-3	200	138.6	50	2	3.5	3.7%

The comparisons of measured and predicted transmission loss of silencer S-1 under pure tone sound excitations at $M = 0$ and 0.051 are shown in Figs. 7(a) and (b), respectively. The frequencies and amplitudes of high amplitude excitations are presented in the tables within Fig. 7, and the low amplitude excitation (linear) is a sinusoidal pulse signal[17] with 20 Pa and 4000 Hz. It can be seen that the predictions agree well with the measurements, except for the differences around the first peak in Fig. 7(b) which may be caused by the additional disturbance of flow in the impedance tube.

In order to validate the 3D time-domain CFD approach for the transmission loss prediction of perforated tube silencer under high amplitude multi-tone sound excitations in the presence of flow, the silencer S-2 is considered. The transmission loss of silencer S-2 has been measured by Chang et al.[12] Because it is difficult to achieve an ideally non-reflecting outlet, Chang et al.[12] installed a long tube downstream of the silencer and measured the acoustic signals in the time period that is not polluted by the reflected signal. The measurement procedure was as follows:

1) First, the tube was connected without the silencer. The flow velocity was set to the desired value, the acoustic signal was adjusted to the required level and the signal from the microphone was captured by the analyzer. This signal represented the acoustic waveform incident on the silencer.

2) Next, the flow was turned off, and the silencer was installed. The flow was set to the same mean velocity as before, and the microphone signal was again recorded. The second signal represents the waveform transmitted through the silencer. Therefore, transmission loss was determined by the differences between the measured incident sound signal without a silencer and the transmitted sound signal with a silencer.

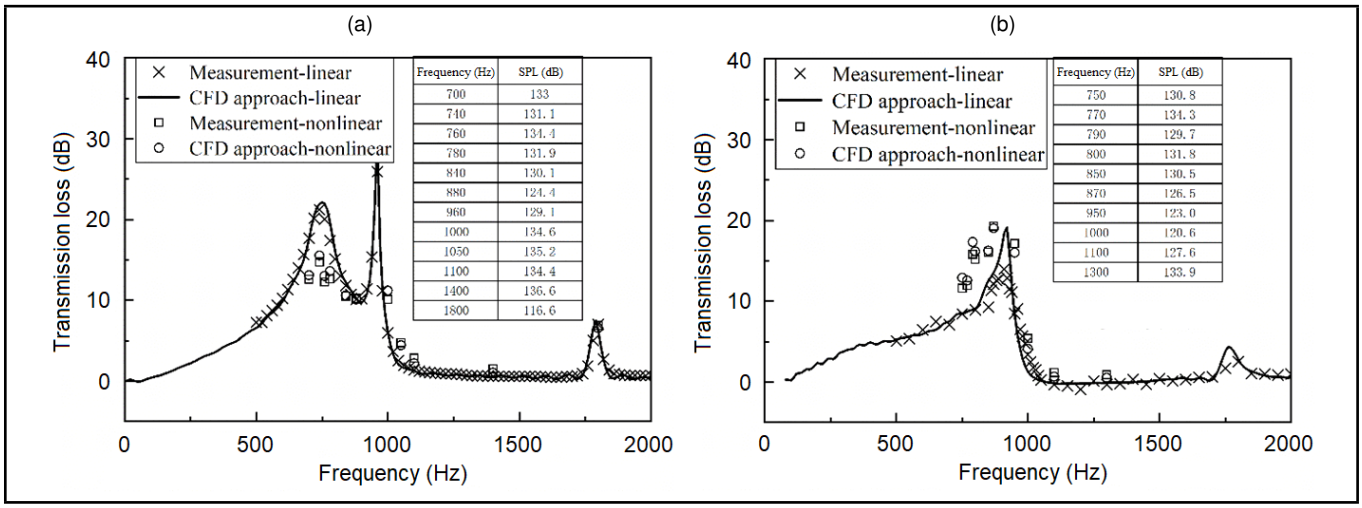

Figure 7. Transmission loss of silencer S-1: (a) $M = 0$, (b) $M = 0.051$.

Table 2. Fundamental frequencies and amplitudes of multi-tone sound excitations.

Order	1	2	3	4	5	6	7	8	9	10
$M = 0.018$	151.7	149.6	146.1	144.8	134.8	135.4	140.8	136.8	124.1	126.3
$M = 0.193$	151.7	149.4	144.6	144.9	139.8	140.3	137.6	137.4	135.5	132.9

The comparisons of predictions and measurements[12] are shown in Figs. 8(b) and (d), and the incident sound pressures are shown in Figs. 8(a) and (c). The fundamental frequencies and amplitudes of high amplitude multi-tone incident sound excitations are presented in Table 2. At $M = 0.018$, the predictions agree well with the measurements at the first seven frequencies, and deviations appear at the others frequencies. The measured transmission loss of silencer S-2 was obtained by calculating the differences of sound powers downstream of the impedance tube with and without the silencer,[12] which is different from the method employed in the present CFD simulation. Therefore the extra nonlinear distortion of high amplitude wave in simulation causes the deviations at the high frequencies whose sound pressure amplitudes are less than that at low frequencies. At $M = 0.193$, obvious deviations are observed at the fifth, seventh and tenth frequencies, which may be caused by the deviations of unsteady flow between the numerical simulation and measurement in the presence of high speed flow. Generally speaking, the acoustic attenuation behavior of perforated tube silencers under the high amplitude sound excitations can be well captured by the 3D time-domain CFD approach.

4. RESULTS AND ANALYSIS

4.1. Transmission Loss Under Pure Tone Sound Excitations

The 3D time-domain CFD approach is applied to calculate the transmission loss of silencer S-3 under the pure tone sound excitations with different SPLs. The predictions at $M = 0$, 0.05, 0.1 and 0.15 are shown in Figs. 9(a), (b), (c) and (d), respectively. Due to the limitation of the loudspeakers, the transmission loss in linear region is measured only. For the situations with low SPLs (linear behavior), the silencer S-3 contributes mainly a broadband resonance, a narrow-band resonance and a low-peak dome attenuation in turn within 2000 Hz, and the pass frequency is near $f = c/(2L)$ at $M = 0$. At $M = 0.05$, the broadband resonance shifts to higher frequency, while the narrow-band resonance disappears and the pass frequency is nearly unchanged. With the Mach number M further increasing, the resonance transforms into the dome attenuation, and the original dome attenuation in higher frequency range is enhanced, gradually. For the cases with high SPLs (nonlinear behavior), the peak of the broadband resonance decreases and gradually becomes a smoothed dome attenuation with an increasing of SPL at $M = 0$. The effect of high amplitude sound weakens with the increasing of M. At $M = 0.15$, even the 155 dB sound excitation cannot generate an obvious nonlinear effect on the acoustic attenuation behavior of silencer S-3. Both high speed flow[26] and high amplitude excitation[29] may lead to the increase of acoustic resistance of perforations, which cause the similar variation trend of transmission loss shown in Figs. 9(a) and (c); however, the mechanisms are different. The acoustic impedance of the orifice is affected by vortex-sound interaction under high speed grazing flow and shedding vortices induced by the high sound particle velocity under high amplitude excitation, respectively.

The sound vorticity $\boldsymbol{\omega}$ is defined as

$$\boldsymbol{\omega} = \omega_x \mathbf{e}_x + \omega_y \mathbf{e}_y + \omega_z \mathbf{e}_z = \nabla \times \mathbf{v}; \tag{5}$$

where $\mathbf{e}_x$, $\mathbf{e}_y$ and $\mathbf{e}_z$ are the components of unit vector, and $\mathbf{v}$ is the vector of acoustic particle velocity.

The normalized y-direction component of vorticity amplitude $|\omega_y| d_h/c$ in the silencer S-3 derived from the CFD computations (800 Hz and 150 dB) at $M = 0$, 0.05, 0.1 and 0.15 are shown in Figs. 10(a), (b), (c) and (d), respectively. Along the axis direction of silencer S-3, the $|\omega_y| d_h/c$ around the orifices decreases gradually. Therefore the acoustic nonlinearity of the orifices weakens with the SPL decreasing in the silencer. When $M = 0$, the vortices are approximately symmetrical along the axis of the orifices. But with the M increasing, the symmetry disappears, and the shedding vortices are restricted to the region near perforations because of the transport of flow.

The axial particle velocities amplitude in the middle of orifices are shown in Fig. 11. From the inlet to the outlet of the silencer S-3, the orders of the axial orifices are ranked from 1

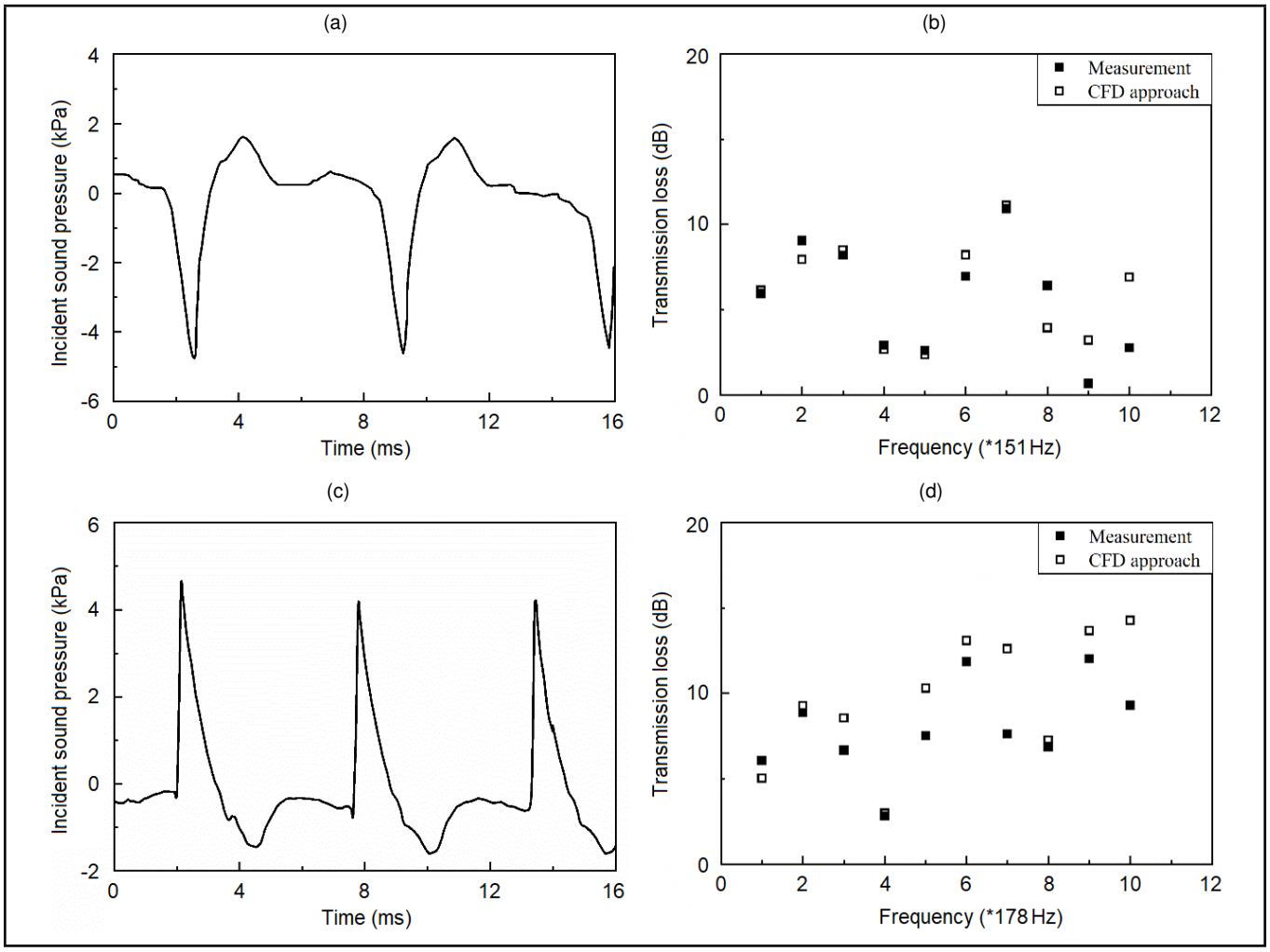

Figure 8. Transmission loss of silencer S-2: (a) incident sound pressure at $M = 0.018$, (b) transmission loss at $M = 0.018$, (c) incident sound pressure at $M = 0.193$, (d) transmission loss at $M = 0.193$.

to 9. It can be seen that the axial particle velocity amplitude in the middle of orifices decreases along the axis of silencer S-3, and the axial particle velocities have no significant variations in the presence of flow.

4.2. Transmission Loss Under Multi-Tone Sound Excitations

In order to investigate the influence of the high amplitude multi-tone sound on the acoustic attenuation behavior of the perforated tube silencer, the 3D time-domain CFD approach is applied to calculate the transmission loss of silencer S-3. The multi-tone sound excitations are enforced on the inlet of silencer S-3 by the form expressed as:

$$p(t) = |p| \sum_{i=1}^{10} \sin(200i * 2\pi t); \tag{6}$$

where $|p|$ is amplitude of the sound pressure at every frequency, t is the time. The transmission loss predictions of silencer S-3 at $M = 0$, 0.05, 0.1 and 0.15 are depicted in Figs. 12(a), (b), (c) and (d), respectively (the values in the legends are the SPLs at the corresponding frequencies). The nonlinear effect on acoustic attenuation behavior of silencer S-3 under multi-tone sound excitation becomes more remarkable than that under pure tone sound excitation, and the influence of multi-tone sound excitation on the transmission loss of the silencer decreases with the increasing of M.

5. CONCLUSIONS

The 3D time-domain CFD approach by solving RANS equations has been employed to predict and analyze acoustic attenuation behaviors of the straight through perforated tube silencers under high amplitude sound excitations in the presence of flow, and the accuracy of the approach was validated by comparing predicted and measured transmission loss of silencers.

Transmission loss of a straight through perforated tube silencer under 110 dB (linear behavior), 140 dB, 150 dB and 155 dB at $M = 0$, 0.05, 0.1 and 0.15 were predicted, respectively. The predictions showed that the transmission loss of the perforated tube silencer was affected significantly by high amplitude sound at low Mach number, and the acoustic nonlinearity weakened with the increased Mach number. With decreased SPL in the silencer, the orifices along the axis direction exhibited weakened acoustic nonlinearity. The effect of multi-tone sound excitation on the transmission loss of the perforated tube silencer was more obvious than the pure tone sound excitation enforced alone, especially near the resonance peak.

The straight through perforated tube silencers investigated in the present work are axisymmetric structures where the cir-

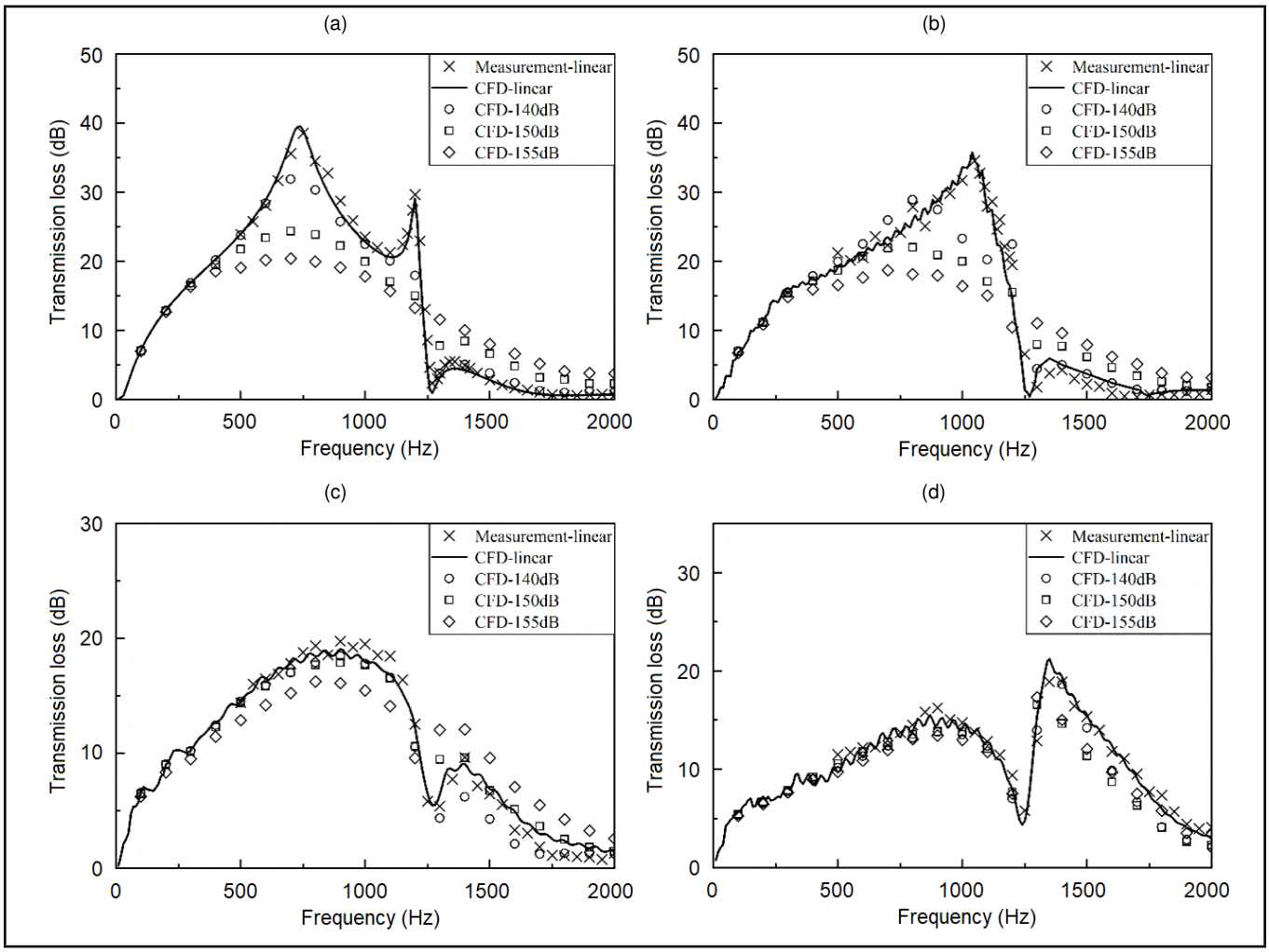

Figure 9. Transmission loss of silencer S-3 under pure tone sound excitations: (a) $M = 0$, (b) $M = 0.05$, (c) $M = 0.1$, (d) $M = 0.15$.

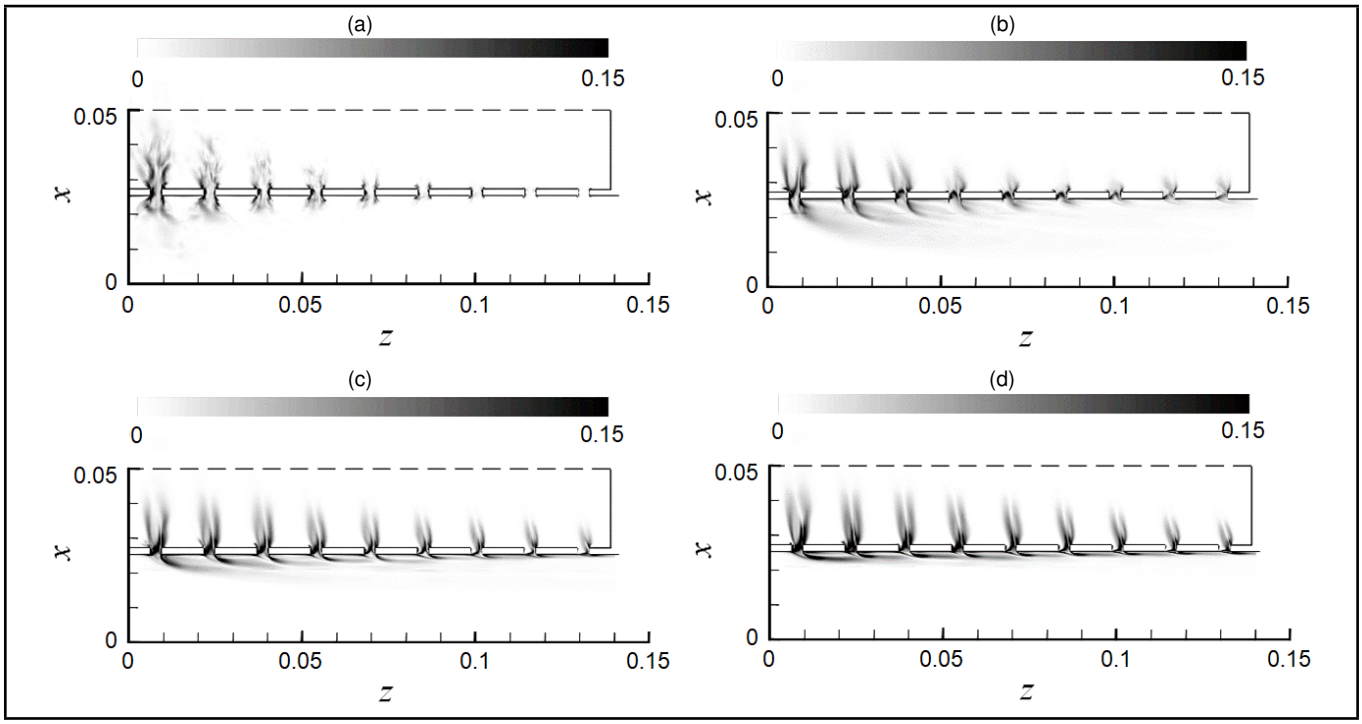

Figure 10. The normalized vorticity amplitude fields in y-direction at 800 Hz and 150 dB, $|\omega_y|d_h/c$: (a) $M = 0$, (b) $M = 0.05$, (c) $M = 0.1$, (d) $M = 0.15$.

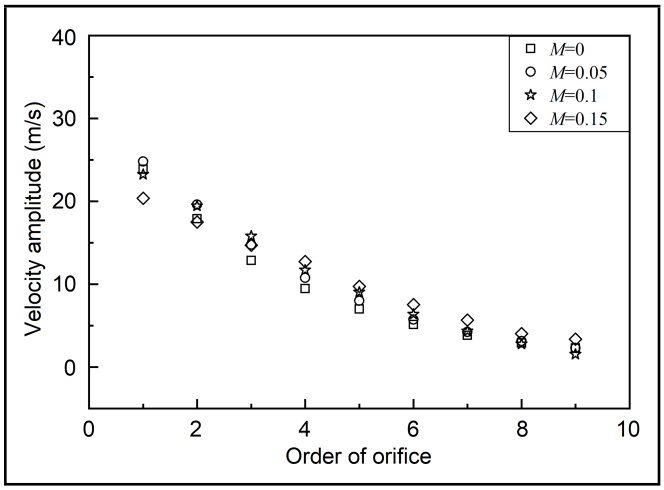

Figure 11. The axial particle velocity amplitude in the middle of orifices at 800 Hz and 150 dB sound excitation.

cumferential modes disappear. Therefore, the rotational periodic boundary condition was adopted to reduce computation time. For an arbitrary-shape silencer, the entire model should be created in computation to consider the effects of 3D waves.

ACKNOWLEDGMENTS

This work was supported by the National Natural Science Foundation of China [grant number 11674076] and the Key Science and Technology Program of Guangxi, China.

REFERENCES

[1] Munjal, M. L. *Acoustic of Ducts and Mufflers*, Wiley, New York, (2014).

[2] Sacks, M. P. and Allen, D. L. Effects of high-intensity sound on muffler element performance, *The Journal of the Acoustical Society of America*, **52** (3A), 725–731, (1972). https://doi.org/10.1121/1.1913167

[3] Ji, Z. L. Acoustic attenuation characteristics of straight-through perforated tube silencers and resonators, *Journal of Computational Acoustics*, **16** (03), 361–379, (2008). https://doi.org/10.1142/S0218396X08003622

[4] Zou, S. G., Wei, K. J., and Wu, X. D. Multi-objective optimization of a multi-chamber perforated muffler using an approximate model and genetic algorithm, *International Journal of Acoustics and Vibration*, **21** (02), 152–163, (2016). https://doi.org/10.20855/ijav.2016.21.2405

[5] Fan Y, Y. L. and Ji, Z. L. Acoustic attenuation performance of two-pass perforated hybrid mufflers with mean flow, *International Journal of Acoustics and Vibration*, **26** (04), 306–315, (2021). https://doi.org/10.20855/ijav.2021.26.41804

[6] Goldman, A. L. Measurement of the acoustic impedance of an orifice under a turbulent boundary layer, *The Journal of the Acoustical Society of America*, **60** (6), 1397–1404, (1976). https://doi.org/10.1121/1.381233

[7] Zhang, Q. and Bodony, D. J. Numerical investigation and modelling of acoustically excited flow through a circular orifice backed by a hexagonal cavity, *Journal of Fluid Mechanics*, **693**, 367–401, (2012). https://doi.org/10.1017/jfm.2011.537

[8] Zhang, Q. and Bodony, D. J. Numerical investigation of a honeycomb liner grazed by laminar and turbulent boundary layers, *Journal of Fluid Mechanics*, **792**, 936–980, (2016). https://doi.org/10.1017/jfm.2016.79

[9] Chen, C., Li, X. D., and Hu, F. Q. On spatially varying acoustic impedance due to high sound intensity decay in a lined duct, *Journal of Sound and Vibration*, **483** (1), 115430, (2020). https://doi.org/10.1016/j.jsv.2020.115430

[10] Sullivan, J. W. A method for modeling perforated tube muffler components. II. Applications, *The Journal of the Acoustical Society of America*, **66** (3), 779–788, (1979). https://doi.org/10.1121/1.383680

[11] Dickey, N. S., Selamet, A., and Novak, J. M. The effect of high-amplitude sound on the attenuation of perforated tube silencers, *The Journal of the Acoustical Society of America*, **108** (3), 1068–1081, (2000). https://doi.org/10.1121/1.1287707

[12] Chang, I. J. and Cummings, A. A time domain solution for the attenuation, at high amplitudes, of perforated tube silencers and comparison with experiment, *Journal of Sound and Vibration*, **122** (2), 243-259, (1988). https://doi.org/10.1016/S0022-460X(88)80352-3

[13] Abd El-Rahman, A. I., Sabry, A. S., and Mobarak, A. Non-linear simulation of single pass perforated tube silencers based on the method of characteristics, *Journal of Sound and Vibration*, **278** (1–2), 63-8, (2004). https://doi.org/10.1016/j.jsv.2003.09.062

[14] Broatch, A., Margot, X., Gil, A., and Denia, F. D. A CFD approach to the computation of the acoustic response of exhaust mufflers, *Journal of Computational Acoustics*, **13** (02), 301–316, (2005). https://doi.org/10.1142/S0218396X05002682

[15] Ji, Z. L., Xu, H. S., and Kang, Z. X. Influence of mean flow on acoustic attenuation performance of straight-through perforated tube reactive silencers and resonators, *Noise Control Engineering Journal*, **58** (1), 12–17, (2010). https://doi.org/10.3397/1.3244593

[16] Liu, C. and Ji, Z. L. Computational fluid dynamics-based numerical analysis of acoustic attenuation and flow resistance characteristics of perforated tube silencers, *Journal of Vibration and Acoustics*, **136** (2), 021006, (2014). https://doi.org/10.1115/1.4026137

[17] Zhu, D. D. and Ji, Z. L. Transmission loss prediction of reactive silencers using 3-D time-domain CFD approach and plane wave decomposition technique, *Applied Acoustics*, **112**, 25–31, (2016). https://doi.org/10.1016/j.apacoust.2016.05.004

[18] Tam, C. K. W., Pastouchenko, N. N., Jones, M. G., and Watson, W. R. Experimental validation of numerical simulations for an acoustic liner in grazing flow: Self-noise and added drag, *Journal of*

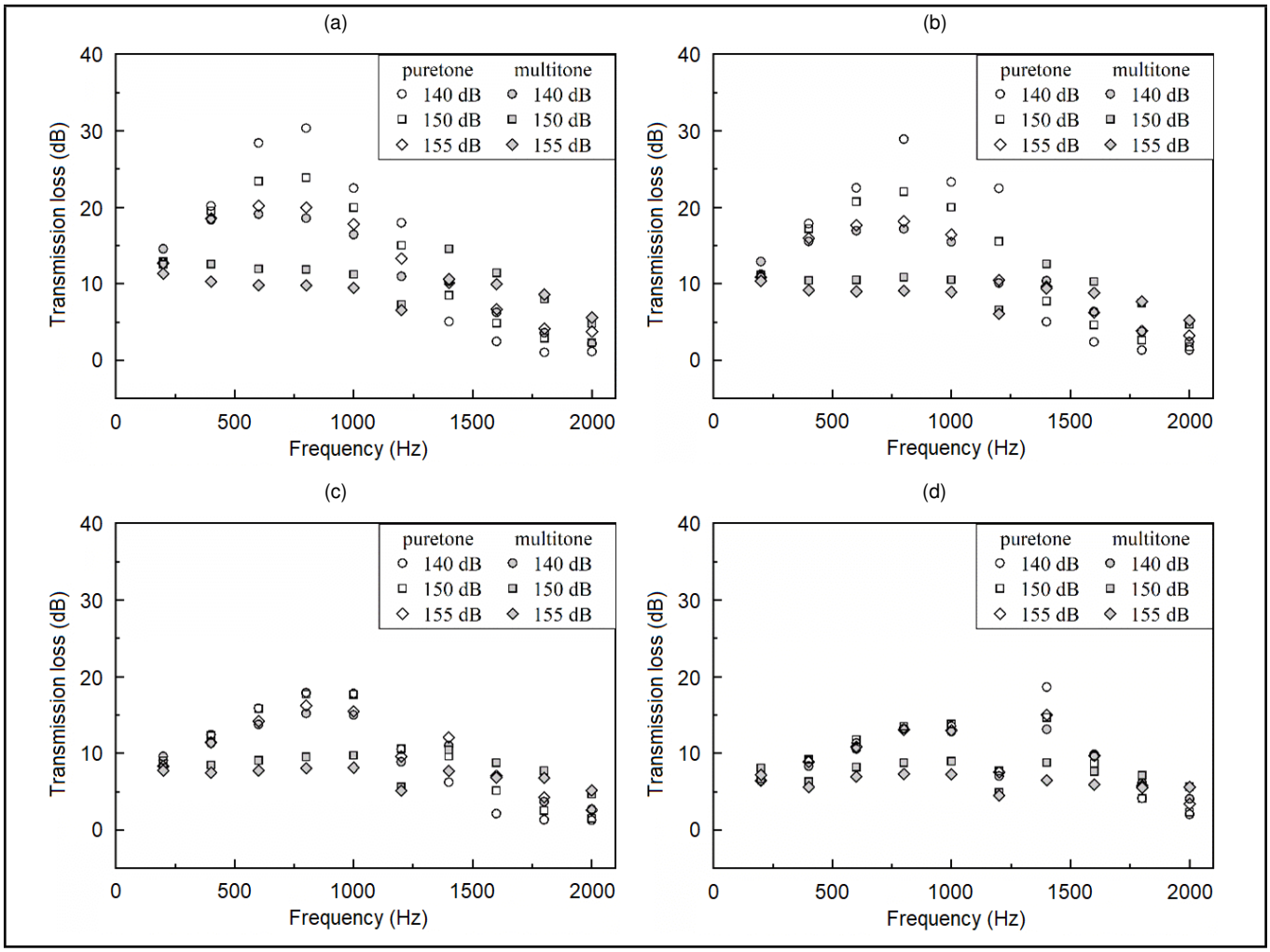

Figure 12. Transmission loss of silencer S-3 under $|p|$ at different SPLs: (a) $M = 0$, (b) $M = 0.05$, (c) $M = 0.1$, (d) $M = 0.15$.

Sound and Vibration, **333** (13), 2831–2854, (2014). https://doi.org/10.1016/j.jsv.2014.02.019

[19] Fan, W. and Guo, L. X. An investigation of acoustic attenuation performance of silencers with mean flow based on three-dimensional numerical simulation, *Shock and Vibration*, **2016**, (2016). https://doi.org/10.1155/2016/6797593

[20] Zhang, H., Fan, W., and Guo, L. X. A CFD results-based approach to investigating acoustic attenuation performance and pressure loss of car perforated tube silencers, *Applied Sciences*, **8** (4), 545, (2018). https://doi.org/10.3390/app8040545

[21] Liu, L. Y., Zheng, X., Hao, Z. Y., and Qiu, Y. A computational fluid dynamics approach for full characterization of muffler without and with exhaust flow, *Physics of Fluids*, **32** (6), (2020). https://doi.org/10.1063/5.0008340

[22] Liu, L. Y., Hao, Z. Y., and Zheng, X. A modified time domain approach for calculation of noise reduction and acoustic impedance of intake duct system, *Applied Acoustics*, **168**, 107420, (2020). https://doi.org/10.1016/j.apacoust.2020.107420

[23] Liu, L. Y., Zheng, X., Hao, Z. Y., and Qiu, Y. A time-domain simulation method to predict insertion loss of a dissipative muffler with exhaust flow, *Physics of Fluids*, **33** (6), (2021). https://doi.org/10.1063/5.0056316

[24] Roche, J. M., Vuillot, F., Leylekian, L., and Delattre, G. Numerical and experimental study of Resonant liners aeroacoustic absorption under grazing flow, *Proc. of the 16th AIAA/CEAS Aeroacoustics Conference*, (2010). https://doi.org/10.2514/6.2010-3767

[25] ANSYS Inc, ANSYS Fluent 18.0 User's Guide, New York, USA, (2018).

[26] Chen, Z. X., Ji, Z. L., and Huang, H. P. Acoustic impedance of perforated plates in the presence of fully developed grazing flow, *Journal of Sound and Vibration*, **485**, 115547, (2020). https://doi.org/10.1016/j.jsv.2020.115547

[27] White, F. M. and Majdalan, J. *Viscous Fluid Flow*, McGraw-Hill, New York, (2006), Chapter 3.

[28] Allam, S. and øAbom, M. Investigation of damping and radiation using full plane wave decomposition in ducts, *Journal of Sound and Vibration*, **292** (3), 519–534, (2006). https://doi.org/10.1016/j.jsv.2005.08.016

[29] Han, K. J., Ji, Z. L., and Fan, Y. L. Extraction and characteristic analysis of the nonlinear acoustic impedance of circular orifices, *Physics of Fluids*, **35** (9), 093606, (2023). https://doi.org/10.1063/5.0166246